Available online at www.sciencedirect.com

ScienceDirect

International Journal of Solids and Structures 45 (2008) 3107–3121

INTERNATIONAL JOURNAL OF SOLIDS AND STRUCTURES

www.elsevier.com/locate/ijsolstr

Buckling of a stiff thin film on a compliant substrate in large deformation

J. Song [a], H. Jiang [b], Z.J. Liu [c], D.Y. Khang [d], Y. Huang [e,*], J.A. Rogers [d], C. Lu [c], C.G. Koh [f]

[a] *Department of Mechanical Science and Engineering, University of Illinois at Urbana-Champaign, Urbana, IL 61801, USA*
[b] *Department of Mechanical and Aerospace Engineering, Arizona State University, Tempe, AZ 85287, USA*
[c] *Institute of High Performance Computing, 1 Science Park Road, #01-01 The Capricorn, Singapore Science Park II, Singapore 117528, Singapore*
[d] *Department of Materials Science and Engineering, Beckman Institute, and Seitz Materials Research Laboratory, University of Illinois at Urbana-Champaign, Urbana, IL 61801, USA*
[e] *Department of Civil and Environmental Engineering and Department of Mechanical Engineering, Northwestern University, Evanston, IL 60208, USA*
[f] *Department of Civil Engineering, National University of Singapore, 1 Engineering Drive 2, E1A 07-03, Singapore 117576, Singapore*

Received 29 September 2007; received in revised form 20 December 2007
Available online 1 February 2008

Abstract

A finite-deformation theory is developed to study the mechanics of thin buckled films on compliant substrates. Perturbation analysis is performed for this highly nonlinear system to obtain the analytical solution. The results agree well with experiments and finite element analysis in wavelength and amplitude. In particular, it is found that the wavelength depends on the strain. Based on the accurate wavelength and amplitude, the membrane and peak strains in thin films, and stretchability and compressibility of the system are also obtained analytically.

Keywords: Finite deformation; Buckling; Thin film; Perturbation analysis; Finite element analysis

1. Introduction

The pioneering work of Bowden et al. (1998) showed that the buckling of stiff thin films on compliant substrates can be controlled in micro and nanoscale systems to generate interesting structures with well defined geometries and dimensions in the 100 nm–100 μm range. This has generated numerous theoretical and experimental studies of the buckling of stiff thin film/compliant substrate systems (e.g., Huang and Suo, 2002; Harrison et al., 2004; Huang, 2005; Huang et al., 2005; Chen and Hutchinson, 2004; Lacour et al., 2004, 2006; Stafford et al., 2004, 2006; Khang et al., 2006; Sun et al., 2006a,b; Choi et al., 2007; Jiang et al., 2007) because

* Corresponding author. Tel.: +1 847 467 3165; fax: +1 847 491 4011.
E-mail address: y-huang@northwestern.edu (Y. Huang).

0020-7683/$ - see front matter © 2008 Elsevier Ltd. All rights reserved.
doi:10.1016/j.ijsolstr.2008.01.023

such systems have important applications in stretchable electronics (Khang et al., 2006; Sun et al., 2006a,b; Choi et al., 2007; Jiang et al., 2007; Wagner et al., 2004), micro and nanoelectromechanical systems (MEMS and NEMS) (Fu et al., 2006), tunable phase optics (Harrison et al., 2004; Efimenko et al., 2005), force spectroscopy in cells (Harris et al., 1980), biocompatible topographic matrices for cell alignment (Jiang et al., 2002; Teixeira et al., 2003), high precision micro and nano-metrology methods (Stafford et al., 2004, 2006; Wilder et al., 2006), and pattern formation for micro/nano-fabrication (Bowden et al., 1998, 1999; Huck et al., 2000; Sharp and Jones, 2002; Yoo et al., 2002; Schmid et al., 2003; Moon et al., 2007). In these systems, controlled buckling is realized in thin films deposited onto prestrained elastomeric substrates. Releasing the prestrain in substrates leads to buckling of thin films.

Fig. 1 illustrates the fabrication of buckled stiff thin films on compliant substrates (Khang et al., 2006; Jiang et al., 2007). Here, thin ribbons of single crystal silicon are chemically bonded to flat, prestrained elastomeric substrates of poly(dimethylsiloxane) (PDMS). The ribbon is along the [1 0 0] direction, and its free surface is (0 1 0). Releasing the prestrain leads to compressive strains on the ribbons that generate the wavy layouts (Khang et al., 2006; Jiang et al., 2007). Such a structure is of interest for applications in stretchable electronics. Field-effect transistors, p–n diodes, and other devices for electronic circuits can be directly integrated into the wavy Si to yield fully stretchable components. Integrated electronics that use such components could be important for devices such as flexible displays (Crawford, 2005), eye-like digital cameras (Jin et al., 2004), conformable skin sensors (Lumelsky et al., 2001), intelligent surgical gloves (Someya et al., 2004), and structural health monitoring devices (Nathan et al., 2000).

For a stiff thin film of thickness h_f and elastic modulus E_f on a pre-stretched (prestrain, ε_{pre}), compliant substrate of modulus E_s, $E_f \gg E_s$, the previous mechanics model (Huang, 2005; Huang et al., 2005; Chen and Hutchinson, 2004) based on the small deformation theory gives a constant wavelength $\lambda_0 = 2\pi h_f[\overline{E}_f/(3\overline{E}_s)]^{1/3}$ of the buckled film and amplitude $A_0 = h_f\sqrt{\varepsilon_{\text{pre}}/\varepsilon_c - 1}$, where $\overline{E}_f = E_f/(1-\nu_f^2)$ and

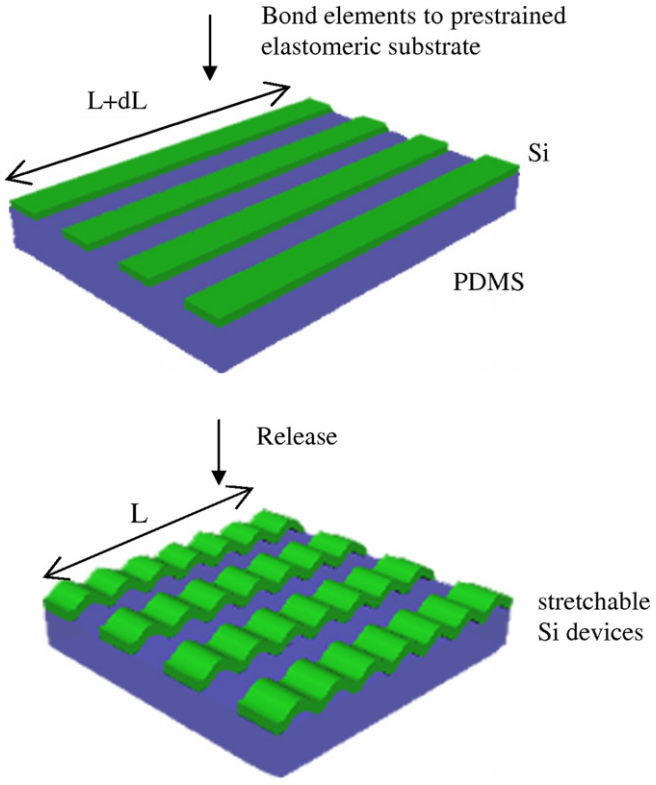

Fig. 1. Schematic illustration of the process for fabricating buckled, or 'wavy', single crystal Si ribbons (green) on a PDMS (blue) substrate. (For interpretation of the references in colour in this figure legend, the reader is referred to the web version of this article.)

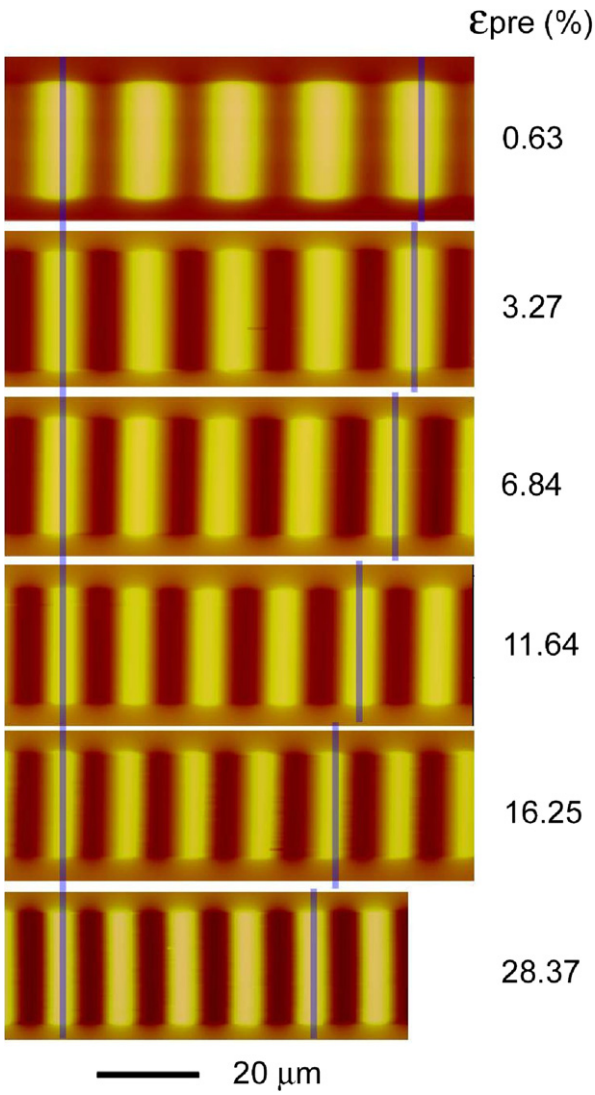

Fig. 2. Optical micrographs of buckled Si ribbons (100 nm thickness) on PDMS, formed with various prestrains (indicated on the right, in percent). The wavelength systematically decreases as the prestrain ε_{pre} increases.

$\overline{E}_s = E_s/(1-v_s^2)$ are plane strain modulus, $\varepsilon_c = \frac{1}{4}(3\overline{E}_s/\overline{E}_f)^{2/3}$ is defined as the critical buckling strain, or the minimum strain needed to induce buckling, which is 0.034% using the literature values for the mechanical properties ($E_f = 130$ GPa, $v_f = 0.27$,[1] $E_s = 1.8$ MPa, $v_s = 0.48$) (Wilder et al., 2006; INSPEC, 1988). The recent experiments at large strains (Khang et al., 2006 and Jiang et al., 2007) show a qualitative behavior characterized by a clear and systematic decrease in wavelength with increasing prestrain as shown in Fig. 2. This strain dependent wavelength behavior has also been reported for layers of polystyrene (PS) on PDMS substrates when the prestrain varies from ~0% to 10% (Harrison et al., 2004), and in platinum films on rubber substrates for prestrains of ~400% (Volynskii et al., 2000). Jiang et al. (2007) pointed out that the strain dependent wavelength is due to the finite deformation (i.e., large strain) in the compliant substrate.

[1] Here, the Young's modulus ($=1/s_{11}$) and Poisson's ratio ($-s_{12}/s_{11}$) are for the [1 0 0] direction of single crystal Si, where s_{ij} are the elastic compliances.

This paper focuses on the buckling analysis of this class of systems illustrated in Fig. 1, although the basic theoretical considerations apply to all related systems in which buckling occurs. We establish a buckling theory that accounts for finite deformations and geometrical nonlinearities to yield a quantitatively accurate description of the system. The analytical solution is obtained via the perturbation method and the numerical results are obtained via the finite element method for this buckling problem of stiff thin film on compliant substrate. The paper is outlined as follows. The finite deformation analysis for the system of stiff thin film/compliant substrate is described in Section 2. The analytical solution is obtained in Section 3 via the perturbation method, which is confirmed by the finite element method in Section 4. The results are given in Section 5, including the wavelength and amplitude of buckled thin films, membrane and peak strains in films, and stretchability and compressibility of the system.

2. The finite deformation buckling analysis for stiff thin films on compliant substrates

The analysis in this section is different from all previous buckling analyses in the following three aspects.

(i) *Finite geometry change:* The initial strain-free (or stress-free) states are different for the PDMS substrate and Si thin film. As illustrated in Fig. 1, the Si thin film is strain free in the top configuration, but becomes compressed in the bottom configuration. On the contrary, the PDMS substrate is stretched in the top configuration and becomes relaxed in the bottom one. This will be further illustrated in Fig. 3.
(ii) *Finite strain:* The strain-displacement relation in the PDMS substrate becomes nonlinear since the maximum prestrain in the experiments is 28% (Jiang et al., 2007).
(iii) *Constitutive model:* The stress–strain relation in the PDMS substrate becomes nonlinear at the large prestrain.

Fig. 3 further illustrates the controlled buckling in Fig. 1. The top figure shows the initial, strain-free state of the PDMS before stretching at the original length L_0. The middle figure shows the stretched PDMS attached to a strain-free Si thin film. The length of the PDMS becomes $(1+\varepsilon_{\text{pre}})L_0$, which is also the original length of the Si film, where ε_{pre} is the prestrain in the stretched PDMS. Releasing the prestrain buckles the Si film, as illustrated in the bottom figure. The coordinate x_1' in the middle figure is related to x_1 in the top figure by $x_1' = (1+\varepsilon_{\text{pre}})x_1$.

2.1. Thin film

The thin film is modeled as a beam since the wavelength in the film (x_1) direction (about 15 μm) is much larger than the film thickness (0.1 μm). The beam, however, undergoes large rotation once the film buckles. The membrane strain ε_{11} is related to the in-plane displacement u_1 and out-of-plane displacement w by

$$\varepsilon_{11} = \frac{\mathrm{d}u_1}{\mathrm{d}x_1'} + \frac{1}{2}\left(\frac{\mathrm{d}w}{\mathrm{d}x_1'}\right)^2, \tag{1}$$

where x_1' is the coordinate for the strain-free configuration of the film (middle figure, Fig. 3). The deformation is plane-strain if the film width (in the direction normal to x_1' and x_3') is much larger than the buckle wavelength.[2] The strain ε_{11} in the film is small such that the membrane force N_{11} can be related to ε_{11} via the plane-strain modulus $\overline{E}_f$ of the film,

$$N_{11} = \overline{E}_f h_f \varepsilon_{11}. \tag{2}$$

The force equilibrium gives the shear and normal tractions at the film/substrate interface as

[2] Jiang, Khang, Kim, Huang, Xiao and Rogers (Finite width effect of thin films buckling on compliant substrate: Experimental and theoretical studies, submitted for publication) obtained the analytical solution for the stiff thin film of finite width on the compliant substrate. For the film width of 20 μm as in the experiments, the wavelength and amplitude given by the analytical solution for finite width are only a few percent different from the present results based on the plane-strain analysis. However, for much thinner films (width on the order of 100 nm), the wavelength becomes much smaller (less than 50%) than that for wider films.

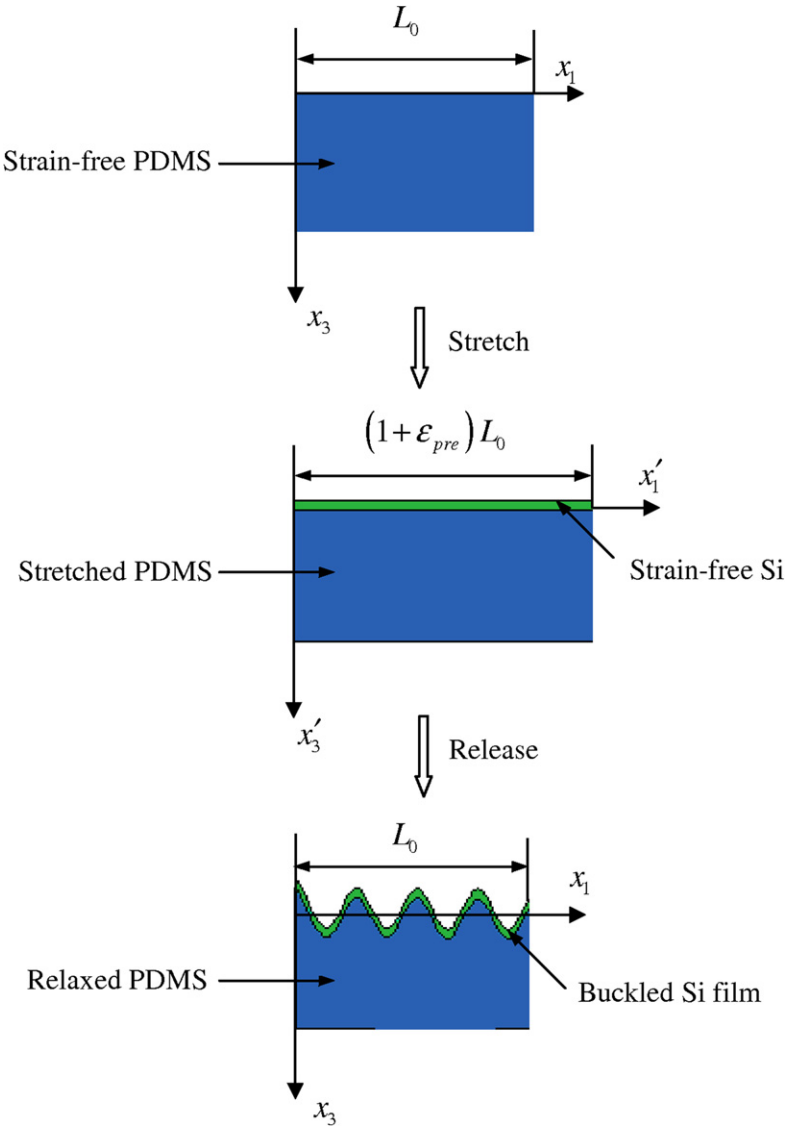

Fig. 3. Three sequential configurations for the thin film/substrate buckling process. The top figure shows the undeformed substrate with the original length L_0, which represents the zero strain energy state. The middle figure shows the substrate deformed by the prestrain and the integrated film, which represents its zero strain energy state. The bottom figure shows the deformed (buckled) configuration.

$$T_1 = \frac{\mathrm{d}N_{11}}{\mathrm{d}x_1'}, \tag{3}$$

and

$$T_3 = -\frac{\overline{E}_f h_f^3}{12}\frac{\mathrm{d}^4 w}{\mathrm{d}x_1'^4} + \frac{\mathrm{d}}{\mathrm{d}x_1'}\left(N_{11}\frac{\mathrm{d}w}{\mathrm{d}x_1'}\right). \tag{4}$$

The strain energy density in the film consists of the membrane energy density, W_m, and bending energy density, W_b, which are given by

$$W_m = \frac{1}{2}N_{11}\varepsilon_{11} = \frac{\overline{E}_f h_f}{2}\varepsilon_{11}^2, \tag{5}$$

and

$$W_b = \frac{\overline{E}_f h_f^3}{24}\left(\frac{\mathrm{d}^2 w}{\mathrm{d}x_1'^2}\right)^2. \tag{6}$$

2.2. Substrate

The substrate is modeled as a semi-infinite solid. The displacements in the substrate are denoted by $u_1(x_1, x_3)$ and $u_3(x_1, x_3)$, where x_1 and x_3 are the coordinates for the strain-free configuration of PDMS substrate (top figure, Fig. 3). For large stretch, the Green strains E_{IJ} in the substrate are related to the displacements as

$$E_{IJ} = \frac{1}{2}\left(\frac{\partial u_I}{\partial x_J} + \frac{\partial u_J}{\partial x_I} + \frac{\partial u_K}{\partial x_I}\frac{\partial u_K}{\partial x_J}\right), \tag{7}$$

where the subscripts I and J are 1 or 3.

The Neo–Hookean constitutive law (Symon, 1971), which is the simplest nonlinear elastic constitutive relation, is used to represent the substrate

$$T_{IJ} = \frac{\partial W_s}{\partial E_{IJ}}, \tag{8}$$

where T_{IJ} is the 2nd Piola–Kirchhoff stress, and the strain energy density W_s takes the form $W_s = \frac{E_s}{6(1-2v_s)}(J-1)^2 + \frac{E_s}{4(1+v_s)}(\overline{I}_1 - 3)$. Here, J is the volume change at a point and is the determinant of deformation gradient F_{iJ}, $\overline{I}_1$ is the trace of the left Cauchy-Green strain tensor $B_{IJ} = F_{Ik}F_{Jk}$ times $J^{-2/3}$, E_s and v_s are the Young's modulus and Poisson's ratio of the substrate, and $E_s = 1.8$ MPa and $v_s = 0.48$ for PDMS (Wilder et al., 2006).

The force equilibrium equation for finite deformation is

$$(F_{iK}T_{JK})_{,J} = 0. \tag{9}$$

and the traction on the surface is $T_i = F_{iK}T_{JK}n_J$, where n_J is the unit normal vector of the surface.

2.3. Buckling analysis

The out-of-plane displacement of the buckled thin film can be represented by

$$w = A\cos\left(\frac{2\pi x_1}{\lambda}\right) = A\cos\left[\frac{2\pi x_1'}{(1+\varepsilon_{\mathrm{pre}})\lambda}\right], \tag{10}$$

in the strain-free configuration (middle figure, Fig. 3) as well as in the relaxed configuration (bottom figure, Fig. 3). Here, the amplitude A and wavelength λ are to be determined.

The bending energy density W_b can be obtained from Eq. (6). The bending energy U_b is the integration of W_b over the length of strain-free thin film, $(1+\varepsilon_{\mathrm{pre}})L_0$ (middle figure, Fig. 3), where L_0 is the length of strain-free PDMS substrate (top figure, Fig. 3). This gives the bending energy U_b as

$$U_b = \frac{\pi^4}{3}\frac{\overline{E}_f h_f^3 A^2}{[(1+\varepsilon_{\mathrm{pre}})\lambda]^4}(1+\varepsilon_{\mathrm{pre}})L_0. \tag{11}$$

The effect of interface shear is negligibly small on the buckling of stiff thin film/compliant substrate system (Huang et al., 2005). The vanishing shear $T_1 = 0$ in Eq. (3) gives the in-plane displacement

$$u_1 = \frac{\pi A^2}{4(1+\varepsilon_{\mathrm{pre}})\lambda}\sin\left[\frac{4\pi x_1'}{(1+\varepsilon_{\mathrm{pre}})\lambda}\right] - \frac{\varepsilon_{\mathrm{pre}}}{1+\varepsilon_{\mathrm{pre}}}x_1', \tag{12}$$

where the last term represents the uniform displacement field in the film if the film does not buckle after the prestretched PDMS is relaxed, and the first term on the right hand side is the axial displacement associated with the buckling.

The membrane strain is

$$\varepsilon_{11} = \frac{\pi^2 A^2}{(1+\varepsilon_{\text{pre}})^2 \lambda^2} - \frac{\varepsilon_{\text{pre}}}{1+\varepsilon_{\text{pre}}}, \tag{13}$$

from which the membrane energy density W_m can be obtained via Eq. (5). The membrane energy U_m is the integration of W_m over the length of strain-free thin film as

$$U_m = \frac{1}{2}\overline{E}_f h_f \left[\frac{\pi^2 A^2}{(1+\varepsilon_{\text{pre}})^2 \lambda^2} - \frac{\varepsilon_{\text{pre}}}{1+\varepsilon_{\text{pre}}}\right]^2 (1+\varepsilon_{\text{pre}}) L_0, \tag{14}$$

where $(1+\varepsilon_{\text{pre}})L_0$ is the length of strain-free thin film (middle figure, Fig. 3).

As shown in the next section, the strain energy density in the substrate is a function of positions x_1 and x_3, as well as the amplitude A and wavelength λ. Its integration over the substrate volume gives the strain energy in the substrate

$$U_s = U_s(A, \lambda), \tag{15}$$

where U_s is proportional to L_0. The amplitude A and wavelength λ are then determined by minimizing the total energy,

$$\frac{\partial}{\partial A}(U_m + U_b + U_s) = \frac{\partial}{\partial \lambda}(U_m + U_b + U_s) = 0. \tag{16}$$

3. Perturbation analysis of the substrate

The deformation in the substrate is highly nonlinear. Since the amplitude A is much smaller than the wavelength λ, we use the perturbation method to expand the displacement field via the power series of the small parameter $\delta = A/\lambda$, i.e.,

$$\begin{cases} u_1(x_1, x_3) = A[u_1^{(0)} + \delta u_1^{(1)} + \delta^2 u_1^{(2)} + \cdots] \\ u_3(x_1, x_3) = A[u_3^{(0)} + \delta u_3^{(1)} + \delta^2 u_3^{(2)} + \cdots] \end{cases}, \tag{17}$$

where $u_1^{(i)}$ and $u_3^{(i)}$ are the ith order, non-dimensional functions to be determined. The Green strain can be similarly expanded as

$$E_{IJ} = A[E_{IJ}^{(0)} + \delta E_{IJ}^{(1)} + \delta^2 E_{IJ}^{(2)} + \cdots], \tag{18}$$

where $E_{IJ}^{(i)}$ is related to the $u_1^{(i)}$ and $u_3^{(i)}$ via Eq. (7) as

$$\begin{aligned} E_{IJ}^{(0)} &= \frac{1}{2}\left(\frac{\partial u_I^{(0)}}{\partial x_J} + \frac{\partial u_J^{(0)}}{\partial x_I}\right) + \frac{A}{2}\frac{\partial u_K^{(0)}}{\partial x_I}\frac{\partial u_K^{(0)}}{\partial x_J} \\ E_{IJ}^{(1)} &= \frac{1}{2}\left(\frac{\partial u_I^{(1)}}{\partial x_J} + \frac{\partial u_J^{(1)}}{\partial x_I}\right) + \frac{A}{2}\left(\frac{\partial u_K^{(0)}}{\partial x_I}\frac{\partial u_K^{(1)}}{\partial x_J} + \frac{\partial u_K^{(0)}}{\partial x_J}\frac{\partial u_K^{(1)}}{\partial x_I}\right) \\ E_{IJ}^{(2)} &= \frac{1}{2}\left(\frac{\partial u_I^{(2)}}{\partial x_J} + \frac{\partial u_J^{(2)}}{\partial x_I}\right) + \frac{A}{2}\left(\frac{\partial u_K^{(0)}}{\partial x_I}\frac{\partial u_K^{(2)}}{\partial x_J} + \frac{\partial u_K^{(0)}}{\partial x_J}\frac{\partial u_K^{(2)}}{\partial x_I} + \frac{\partial u_K^{(1)}}{\partial x_I}\frac{\partial u_K^{(1)}}{\partial x_J}\right) \end{aligned} \tag{19}$$

The 2nd Piola–Kirchhoff stress T_{IJ} can be obtained from the expansion of the constitutive law (Eq. (8)) as

$$
\begin{aligned}
T_{11} &= \frac{E_s}{6(1-2\nu_s)}\begin{pmatrix} 2E_{11}+2E_{33}+2E_{11}E_{33}-3E_{11}^2-4E_{13}^2+E_{33}^2 \\ +4E_{13}^2E_{33}+12E_{11}E_{13}^2-3E_{11}^2E_{33}-E_{11}E_{33}^2+5E_{11}^3-E_{33}^3 \end{pmatrix} \\
&\quad+\frac{E_s}{1+\nu_s}\begin{pmatrix} \frac{2}{3}E_{11}-\frac{2}{3}E_{33}+\frac{4}{9}E_{11}E_{33}-\frac{16}{9}E_{11}^2-2E_{13}^2+\frac{2}{9}E_{33}^2 \\ +\frac{32}{9}E_{13}^2E_{33}+\frac{80}{9}E_{11}E_{13}^2-\frac{8}{9}E_{11}^2E_{33}+\frac{112}{27}E_{11}^3-\frac{8}{27}E_{33}^3 \end{pmatrix}, \\
T_{33} &= \frac{E_s}{6(1-2\nu_s)}\begin{pmatrix} 2E_{11}+2E_{33}+2E_{11}E_{33}-3E_{33}^2-4E_{13}^2+E_{11}^2 \\ +4E_{13}^2E_{11}+12E_{33}E_{13}^2-3E_{33}^2E_{11}-E_{33}E_{11}^2+5E_{33}^3-E_{11}^3 \end{pmatrix} \\
&\quad+\frac{E_s}{1+\nu_s}\begin{pmatrix} \frac{2}{3}E_{33}-\frac{1}{3}E_{11}+\frac{4}{9}E_{11}E_{33}-\frac{16}{9}E_{33}^2-2E_{13}^2+\frac{2}{9}E_{11}^2 \\ +\frac{32}{9}E_{13}^2E_{11}+\frac{80}{9}E_{33}E_{13}^2-\frac{8}{9}E_{33}^2E_{11}+\frac{112}{27}E_{33}^3-\frac{8}{27}E_{11}^3 \end{pmatrix}, \\
T_{13} &= \frac{E_s}{3(1-2\nu_s)}(-2E_{11}E_{13}-2E_{13}E_{33}+3E_{11}^2E_{13}+3E_{13}E_{33}^2+2E_{11}E_{13}E_{33}+4E_{13}^3) \\
&\quad+\frac{E_s}{1+\nu_s}\left(E_{13}-2E_{11}E_{13}-2E_{13}E_{33}+\frac{40}{9}E_{11}^2E_{13}+\frac{40}{9}E_{13}E_{33}^2+\frac{32}{9}E_{11}E_{13}E_{33}+\frac{16}{3}E_{13}^3\right).
\end{aligned}
\tag{20}
$$

The deformation gradient can be expanded as

$$
\begin{aligned}
F_{11} &= 1+\frac{\partial u_1}{\partial x_1} = 1+A\left[\frac{\partial u_1^{(0)}}{\partial x_1}+\delta\frac{\partial u_1^{(1)}}{\partial x_1}+\delta^2\frac{\partial u_1^{(2)}}{\partial x_1}+\cdots\right] \\
F_{13} &= \frac{\partial u_1}{\partial x_3} = A\left[\frac{\partial u_1^{(0)}}{\partial x_3}+\delta\frac{\partial u_1^{(1)}}{\partial x_3}+\delta^2\frac{\partial u_1^{(2)}}{\partial x_3}+\cdots\right] \\
F_{31} &= \frac{\partial u_3}{\partial x_1} = A\left[\frac{\partial u_3^{(0)}}{\partial x_1}+\delta\frac{\partial u_3^{(1)}}{\partial x_1}+\delta^2\frac{\partial u_3^{(2)}}{\partial x_1}+\cdots\right] \\
F_{33} &= 1+\frac{\partial u_3}{\partial x_3} = 1+A\left[\frac{\partial u_3^{(0)}}{\partial x_3}+\delta\frac{\partial u_3^{(1)}}{\partial x_3}+\delta^2\frac{\partial u_3^{(2)}}{\partial x_3}+\cdots\right].
\end{aligned}
\tag{21}
$$

The substitution of Eqs. (19)–(21) into the equilibrium Eq. (9) yields the linear ordinary differential equations for $u_i^{(0)}$, $u_i^{(1)}$, and $u_i^{(2)}$. The boundary conditions are

$$
\begin{aligned}
&T_1 = 0 \quad \text{and} \quad u_3 = A\cos\left(\frac{2\pi x_1}{\lambda}\right) \quad \text{at} \quad x_3 = 0 \\
&T_1 = 0 \quad \text{and} \quad T_3 = 0 \quad \text{at} \quad x_3 = \infty.
\end{aligned}
\tag{22}
$$

The displacement fields $u_i^{(0)}$, $u_i^{(1)}$, and $u_i^{(2)}$ are obtained analytically as

$$
\begin{cases}
u_1^{(0)}(x_1,x_3) = \frac{2\pi}{\lambda}x_3 e^{\frac{-2\pi}{\lambda}x_3}\sin\left(\frac{2\pi}{\lambda}x_1\right) \\
u_3^{(0)}(x_1,x_3) = -\left(1+\frac{2\pi^2}{\lambda}x_3\right)e^{\frac{-2\pi}{\lambda}x_3}\cos\left(\frac{2\pi}{\lambda}x_1\right)
\end{cases},
\tag{23}
$$

$$
\begin{cases}
u_1^{(1)}(x_1,x_3) = \left(\frac{3\pi}{2\lambda}x_3-\frac{1}{8}\right)e^{\frac{-4\pi}{\lambda}x_3}\sin\left(\frac{4\pi}{\lambda}x_1\right) \\
u_3^{(1)}(x_1,x_3) = -\left(\frac{2\pi^2}{\lambda^2}x_3^2+\frac{\pi}{\lambda}x_3\right)e^{\frac{-4\pi}{\lambda}x_3}+\frac{3\pi}{2\lambda}x_3e^{\frac{-4\pi}{\lambda}x_3}\cos\left(\frac{4\pi}{\lambda}x_1\right)
\end{cases},
\tag{24}
$$

and

$$
\begin{cases}
u_1^{(2)}(x_1,x_3) = \left(\frac{13\pi}{64\lambda}x_3-\frac{3}{16}\right)e^{\frac{-2\pi}{\lambda}x_3}\sin\left(\frac{2\pi}{\lambda}x_1\right)+\frac{\pi}{\lambda}x_3e^{\frac{-6\pi}{\lambda}x_3}\sin\left(\frac{6\pi}{\lambda}x_1\right) \\
-\left(\frac{\pi^3}{2\lambda^3}x_3^3+\frac{21\pi^2}{8\lambda^2}x_3^2+\frac{45\pi}{64\lambda}x_3-\frac{5}{16}\right)e^{\frac{-6\pi}{\lambda}x_3}\sin\left(\frac{2\pi}{\lambda}x_1\right) \\
u_3^{(2)}(x_1,x_3) = \left(\frac{13\pi}{64\lambda}x_3-\frac{11}{128}\right)e^{\frac{-2\pi}{\lambda}x_3}\cos\left(\frac{2\pi}{\lambda}x_1\right)+\frac{\pi}{\lambda}x_3e^{\frac{-6\pi}{\lambda}x_3}\cos\left(\frac{6\pi}{\lambda}x_1\right) \\
+\left(\frac{5\pi^3}{2\lambda^3}x_3^3-\frac{29\pi^2}{8\lambda^2}x_3^2-\frac{71\pi}{64\lambda}x_3+\frac{11}{128}\right)e^{\frac{-6\pi}{\lambda}x_3}\cos\left(\frac{2\pi}{\lambda}x_1\right).
\end{cases}
\tag{25}
$$

Here, we have taken the Poisson's ratio $v_s \approx 1/2$ since the substrate is nearly incompressible. The strain energy in the substrate can be obtained by integrating the strain energy density W_s as

$$U_s = \frac{\pi}{3}\frac{E_s A^2}{\lambda}\left(1 + \frac{5}{32}\frac{\pi^2 A^2}{\lambda^2}\right)L_0, \tag{26}$$

where L_0 is the original length of the substrate.

4. Post-buckling analysis

The buckling analysis in Sections 2 and 3 is for the stiff thin film/compliant substrate system subjected to the prestrain. The post-buckling behavior, i.e., the system subjected to the applied strain after buckling, is studied in this section to determine the system stretchability/compressibility. Fig. 4 illustrates the buckled Si thin film and relaxed PDMS substrate of length L_0 (left figure) and the system that is subjected to the applied strain $\varepsilon_{\text{applied}}$ and has the length $(1 + \varepsilon_{\text{applied}})L_0$ (right figure). The coordinate x_1'' in the right figure is related to x_1 in the left figure by $x_1'' = (1 + \varepsilon_{\text{applied}})x_1$. The out-of-plane displacement of the buckled thin film can be represented by

$$w = A'' \cos\left(\frac{2\pi x_1''}{\lambda''}\right) = A'' \cos\left[\frac{2\pi(1 + \varepsilon_{\text{applied}})x_1}{\lambda''}\right], \tag{27}$$

in the relaxed configuration (left figure, Fig. 4) and stretched configuration (right figure, Fig. 4). Here, the amplitude A'' and wavelength λ'' are to be determined in terms of the applied strain $\varepsilon_{\text{applied}}$. In the strain-free configuration x_1' of the thin film (middle figure, Fig. 3), Eq. (27) takes the form

$$w = A'' \cos\left[\frac{2\pi(1 + \varepsilon_{\text{applied}})x_1'}{(1 + \varepsilon_{\text{pre}})\lambda''}\right]. \tag{28}$$

This gives the bending energy in the thin film

$$U_b = \frac{\pi^4}{3}\overline{E}_f h_f^3 A''^2 \left[\frac{1 + \varepsilon_{\text{applied}}}{(1 + \varepsilon_{\text{pre}})\lambda''}\right]^4 (1 + \varepsilon_{\text{pre}})L_0, \tag{29}$$

where $(1 + \varepsilon_{\text{pre}})L_0$ is the length of strain-free thin film (middle figure, Fig. 3).

The vanishing shear $T_1 = 0$ in Eq. (3) gives the in-plane displacement

$$u_1 = \frac{\pi(1 + \varepsilon_{\text{applied}})A''^2}{4(1 + \varepsilon_{\text{pre}})\lambda''} \sin\left[\frac{4\pi(1 + \varepsilon_{\text{applied}})x_1'}{(1 + \varepsilon_{\text{pre}})\lambda''}\right] - \frac{\varepsilon_{\text{pre}} - \varepsilon_{\text{applied}}}{1 + \varepsilon_{\text{pre}}}x_1'. \tag{30}$$

The membrane energy in the thin film becomes

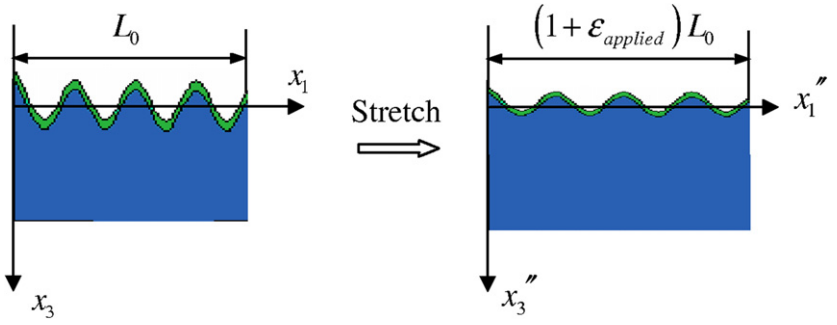

Fig. 4. Schematic illustration of the buckled Si thin film and relaxed PDMS substrate of length L_0 (left figure) and the system that is subjected to the applied strain $\varepsilon_{\text{applied}}$ and has the length $(1 + \varepsilon_{\text{applied}})L_0$ (right figure).

$$U_m = \frac{1}{2}\overline{E}_f h_f \left[\left(\frac{1+\varepsilon_{\text{applied}}}{1+\varepsilon_{\text{pre}}} \right)^2 \frac{\pi^2 A''^2}{\lambda''^2} - \frac{\varepsilon_{\text{pre}} - \varepsilon_{\text{applied}}}{1+\varepsilon_{\text{pre}}} \right]^2 (1+\varepsilon_{\text{pre}}) L_0, \tag{31}$$

where $(1+\varepsilon_{\text{pre}})L_0$ is the once again length of strain-free thin film (middle figure, Fig. 3).

We also use the perturbation method to write the displacement field in the substrate as

$$\begin{cases} u_1(x_1, x_3) = A'' \left[\varepsilon_{\text{applied}} \frac{x_1}{A''} + u_1^{(0)} + \delta u_1^{(1)} + \delta^2 u_1^{(2)} + \cdots \right] \\ u_3(x_1, x_3) = A'' \left[-\frac{\nu_s}{1-\nu_s} \varepsilon_{\text{applied}} \frac{x_3}{A''} + u_3^{(0)} + \delta u_3^{(1)} + \delta^2 u_3^{(2)} + \cdots \right] \end{cases}, \tag{32}$$

where $\delta = A''/\lambda''$ is small, and $u_1^{(i)}$ and $u_3^{(i)}$ are the ith order, non-dimensional functions to be determined via the same approach as Section 3 for the prestrain. For the nearly incompressible substrate $\nu_s \approx 1/2$, the strain energy in the substrate can be obtained as

$$U_s = \frac{\pi}{3} \frac{E_s A''^2}{\lambda''} (1+\varepsilon_{\text{applied}}) \left[1 + \varepsilon_{\text{applied}} + \frac{5}{32} \frac{\pi^2 A''^2}{\lambda''^2} (1+\varepsilon_{\text{applied}})^2 \right] L_0. \tag{33}$$

5. Finite element analysis

The finite element method is used to study the buckling of stiff thin film/compliant substrate system in order to validate the analytical solution given in Section 3. The challenges in the numerical analysis of such systems include:

(1) *Extremely large difference in the film and substrate elastic properties*. The Young's modulus of Si thin film (~100 GPa) is about 5 orders of magnitude larger than the Young's modulus of PDMS substrate (~1 MPa).
(2) *Extremely large difference in the film and substrate thickness*. The film thickness (~100 nm) is about 4 orders of magnitude smaller than the substrate thickness (~1 mm).

These challenges require very fine mesh near the film/substrate interface.

The modeled system consists of a 3.02 mm-thick PDMS substrate and a 100 nm-thick Si thin film. The length of the two-dimensional system is 1 mm. The Si thin film is modeled by the beam elements (B21 in the ABAQUS finite element program, 2004). The substrate is modeled by the 4-node plane-strain element (CPE4) with the smallest element size 0.4 μm × 0.4 μm. Once the substrate is subjected to the prestrain ε_{pre}, its top free surface is attached to the thin film by sharing the film and substrate with the same nodes at the interface. The beam element (B21 in ABAQUS) is compatible with the 2D plane-strain solid elements in the substrate. The rotational degree of freedom in the beam elements is constrained when connected with the plane-strain solid elements.

We first determine the eigenvalues and eigenmodes of the stiff thin film/compliant substrate system. The first eigenmode is then used as initial small geometrical imperfection to trigger the buckling of the system. We have also used the random combination of various buckling modes, and find the results (wavelength and amplitude) to be independent of the modes. The imperfections are always small enough to ensure that the solution is accurate.

6. Results and discussion

6.1. Wavelength and amplitude due to the pre-strain

The total energy consists of the membrane and bending energy in the thin film and the strain energy in the substrate, $U_{\text{total}} = U_m + U_b + U_s$. Minimization of total energy, i.e., $\frac{\partial U_{\text{total}}}{\partial A} = \frac{\partial U_{\text{total}}}{\partial \lambda} = 0$ gives the wavelength and amplitude

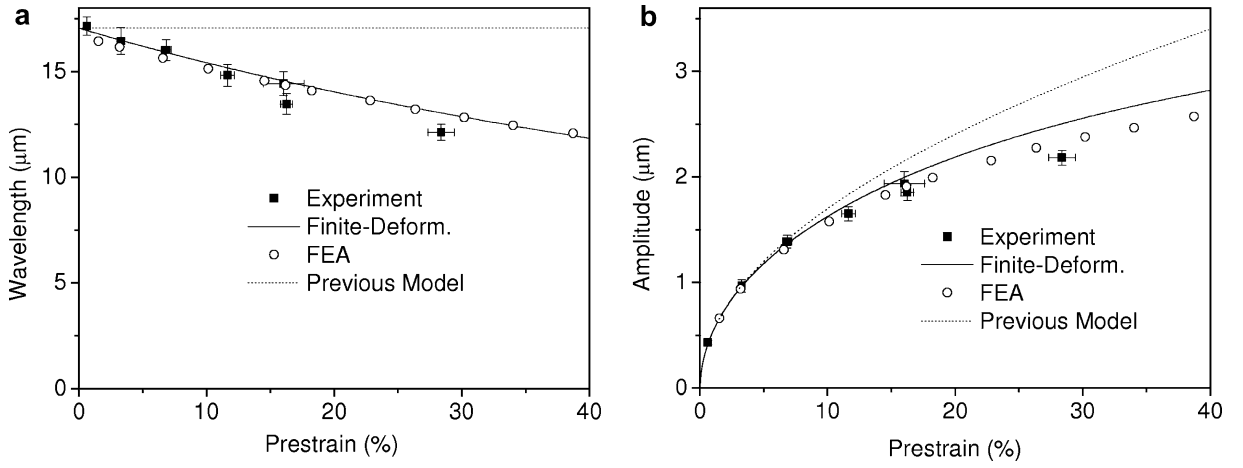

Fig. 5. (a) Wavelength and (b) amplitude of buckled structures of Si (100 nm thickness) on PDMS as a function of the prestrain. The finite-deformation buckling theory yields wavelengths and amplitudes that both agree well with experiments and finite element analysis. Results from previous mechanics models (i.e., small deformation limit) are also shown.

$$\lambda = \frac{\lambda_0}{(1+\varepsilon_{\text{pre}})(1+\xi)^{1/3}}, \quad A \approx \frac{A_0}{\sqrt{1+\varepsilon_{\text{pre}}}(1+\xi)^{1/3}},^{3} \tag{34}$$

where $\lambda_0 = 2\pi h_f[\overline{E}_f/(3\overline{E}_s)]^{1/3}$ and $A_0 = h_f\sqrt{\varepsilon_{\text{pre}}/\varepsilon_c - 1}$ are the wavelength and amplitude based on small deformation theory, and $\xi = 5\varepsilon_{\text{pre}}(1+\varepsilon_{\text{pre}})/32$. As with the previous analyses, the finite deformation theory predicts non-zero amplitude when the prestrain, ε_{pre}, exceeds the critical strain, ε_c. However, the wavelength is different from that given by previous theories due to the large prestrain. As shown in Fig. 5, the wavelength depends on the prestrain, and it agrees well with the experimental data and finite element analysis without any parameter fitting. For small prestrain, λ approaches λ_0.

6.2. Membrane and peak strains in the film due to the pre-strain

For $\varepsilon_{\text{pre}} < \varepsilon_c$ (=0.034% for the Si/PDMS system), relaxing the prestrain does not lead to buckling. Instead, the film supports a small compressive strain $-\varepsilon_{\text{pre}}$, which we refer to as membrane strain. When $\varepsilon_{\text{pre}} > \varepsilon_c$, the film buckles to relieve some of the strain. The membrane strain, ε_{mem}, as evaluated at the plane that lies at the midpoint of the thickness of the film, is obtained from Eq. (13) as $\varepsilon_{\text{mem}} = -\frac{1+\frac{\xi}{3}}{(1+\xi)^{1/3}}\varepsilon_c$. For the prestrain up to 100%, this membrane strain remains essentially a constant, $-\varepsilon_c$. The maximum strain in the film, also called the peak strain $\varepsilon_{\text{peak}}$, is the sum of membrane strain ε_{mem} and the bending strain induced by the buckled geometry. In most cases of practical interest, the strain associated with the buckled geometry is much larger than ε_{mem}, thus this peak strain can be written as

$$\varepsilon_{\text{peak}} = 2\sqrt{\varepsilon_{\text{pre}}\varepsilon_c}\frac{(1+\xi)^{1/3}}{\sqrt{1+\varepsilon_{\text{pre}}}}. \tag{35}$$

The magnitude of $\varepsilon_{\text{peak}}$ is typically much smaller than the overall strain, $\varepsilon_{\text{pre}} - \varepsilon_{\text{mem}}$, that the film accommodates by buckling. For example, in the case of $\varepsilon_{\text{pre}} = 29.2\%$, $\varepsilon_{\text{peak}}$ is only 1.8% for the system of Fig. 1. This mechanical advantage provides an effective level of stretchability/compressibility in materials that are intrinsically brittle. Fig. 6 shows $\varepsilon_{\text{peak}}$ and ε_{mem} as a function of ε_{pre}. Both the membrane and peak strains agree well with finite element analysis. The membrane strain is negligible compared to the peak strain. Likewise, the peak strain is much smaller than the prestrain, such that the system can accommodate large strains. As a result, $\varepsilon_{\text{peak}}$

[3] The exact solution of the amplitude is $A = h_f\frac{\sqrt{\frac{\varepsilon_{\text{pre}}}{\varepsilon_c} - \frac{1+\frac{\xi}{3}}{(1+\xi)^{1/3}}(1+\varepsilon_{\text{pre}})}}{\sqrt{1+\varepsilon_{\text{pre}}}(1+\xi)^{1/3}}$. For $\varepsilon_{\text{pre}} \gg \varepsilon_c$, the numerator is approximately $\sqrt{\frac{\varepsilon_{\text{pre}}}{\varepsilon_c} - 1}$, which gives the amplitude in Eq. (34).

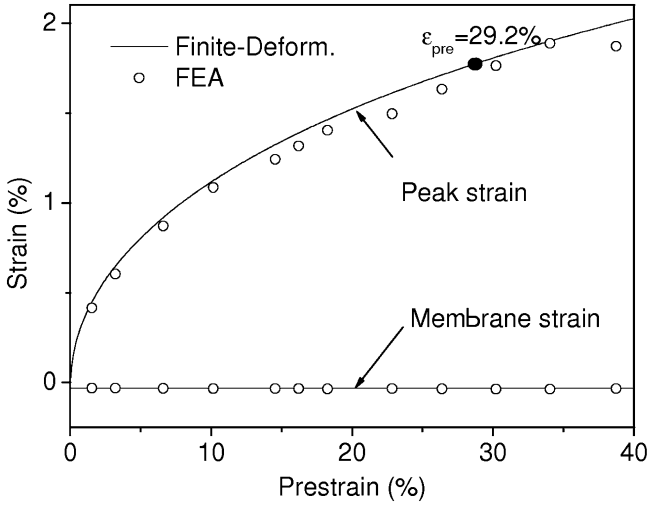

Fig. 6. Membrane and peak strains in the Si as a function of prestrain for a system of buckled Si ribbons (100 nm thickness) on a PDMS substrate. The membrane strain is a small and constant throughout this range.

determines the point at which fracture occurs in the film. For Si, the fracture strain is around $\varepsilon_{\text{fracture}} = 1.8\%$. The maximum allowable prestrain is, therefore, approximately $\frac{\varepsilon_{\text{fracture}}^2}{4\varepsilon_c}\left(1+\frac{43}{48}\frac{\varepsilon_{\text{fracture}}^2}{4\varepsilon_c}\right)$, which, for the system examined here, is ~29% or almost twenty times larger than $\varepsilon_{\text{fracture}}$.

6.3. Stretchability and compressibility due to the applied strain

The minimization of total energy, which is the sum of thin film (membrane and bending) energy and substrate energy in Eqs. (29)–(31) and (33), gives the wavelength and amplitude

$$\lambda'' = \frac{\lambda_0(1+\varepsilon_{\text{applied}})}{(1+\varepsilon_{\text{pre}})(1+\varepsilon_{\text{applied}}+\zeta)^{1/3}}, \quad A'' \approx h_f \frac{\sqrt{(\varepsilon_{\text{pre}}-\varepsilon_{\text{applied}})/\varepsilon_c - 1}}{\sqrt{1+\varepsilon_{\text{pre}}}(1+\varepsilon_{\text{applied}}+\zeta)^{1/3}},^{4} \tag{36}$$

where $\zeta = 5(\varepsilon_{\text{pre}} - \varepsilon_{\text{applied}})(1+\varepsilon_{\text{pre}})/32$. Fig. 7 shows the experimentally measured and theoretically predicted wavelength λ'' and amplitude A'' versus applied strain $\varepsilon_{\text{applied}}$ for a buckled Si thin film/PDMS substrate system formed at the prestrain of 16.2%. The constant wavelength and the amplitude predicted by the previous mechanics models, with ε_{pre} replaced by $\varepsilon_{\text{pre}} - \varepsilon_{\text{applied}}$, are also shown as well as the finite element results. The measured wavelength increases with the applied tensile strain, and the measured amplitude decreases, reaching zero once the applied tensile strain reaches the prestrain. The finite-deformation buckling theory agrees well with experiments and finite element analysis for both amplitude and wavelength. The previous mechanics models also capture the amplitude trend but deviate from the experimental results for large tensile strain (>10%). The amplitude A'' vanishes when the applied strain reaches the prestrain plus the critical strain ε_c. Therefore, the stretchability (maximum applied tensile strain) is $\varepsilon_{\text{pre}} + \varepsilon_{\text{fracture}} + \varepsilon_c$, which varies linearly with the prestrain. The peak strain in the film is

$$\varepsilon_{\text{peak}} = 2\sqrt{(\varepsilon_{\text{pre}}-\varepsilon_{\text{applied}})\varepsilon_c}\frac{(1+\varepsilon_{\text{applied}}+\zeta)^{1/3}}{\sqrt{1+\varepsilon_{\text{pre}}}}. \tag{37}$$

Fig. 8 shows $\varepsilon_{\text{peak}}$ and ε_{mem} as a function of $\varepsilon_{\text{applied}}$. The results predicted by the finite-deformation buckling theory agree well with finite element analysis. The Si film fails once $\varepsilon_{\text{applied}}$ reaches 12.5%. The compressibility

[4] The exact solution of the amplitude is $A'' = h_f \frac{\sqrt{\frac{\varepsilon_{\text{pre}}-\varepsilon_{\text{applied}}}{\varepsilon_c} - \frac{1+\varepsilon_{\text{applied}}+\frac{\zeta}{3}}{(1+\varepsilon_{\text{applied}}+\zeta)^{1/3}}(1+\varepsilon_{\text{pre}})}}{\sqrt{1+\varepsilon_{\text{pre}}}(1+\varepsilon_{\text{applied}}+\zeta)^{1/3}}$. For $\varepsilon_{\text{pre}} - \varepsilon_{\text{applied}} \gg \varepsilon_c$, the numerator is approximately $\sqrt{\frac{\varepsilon_{\text{pre}}-\varepsilon_{\text{applied}}}{\varepsilon_c}} - 1$, which gives the amplitude in Eq. (36).

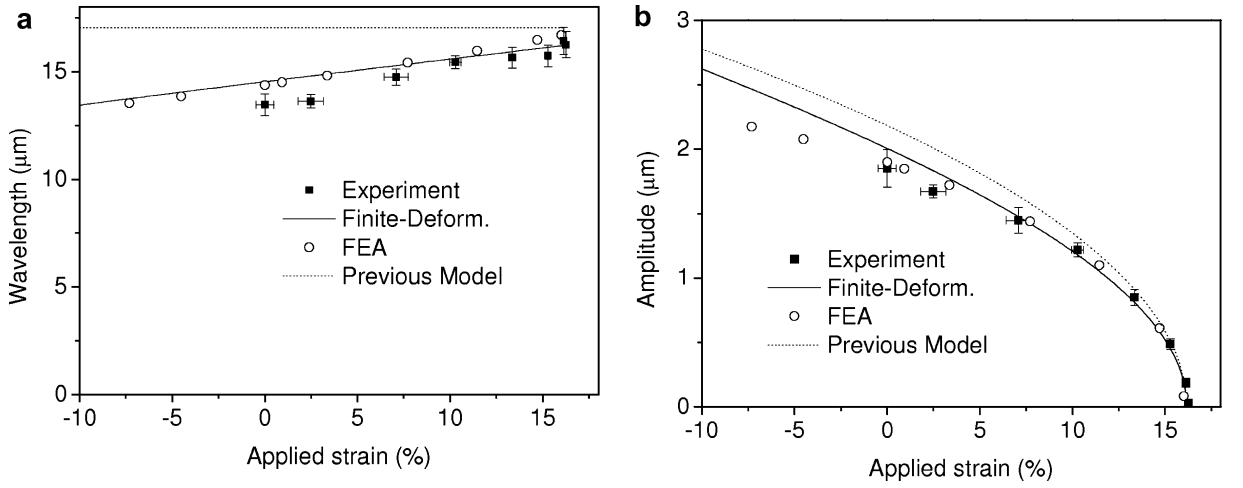

Fig. 7. (a) Wavelength and (b) amplitude of buckled structures of Si (100 nm thickness) on PDMS formed with a prestrain of 16.2%, as a function of the applied strain. The measured wavelength increases for tensile strain and the measured amplitude decreases, reaching zero once the tensile strain reaches the prestrain. The finite-deformation buckling theory yields wavelengths and amplitudes that both agree well with experiments and finite element analysis. Results from previous mechanics models (i.e., small deformation limit) are also shown.

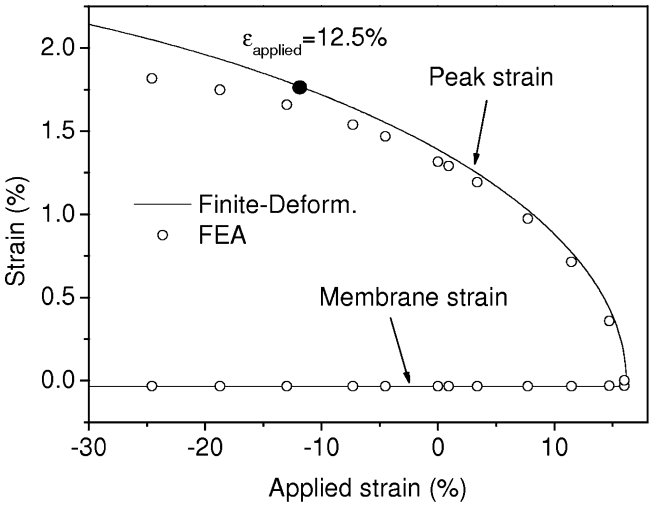

Fig. 8. Membrane and peak strains in the Si as a function of applied strain for a system of buckled Si ribbons (100 nm thickness) on a PDMS substrate with a prestrain of 16.2%.

is the maximum applied compressive strain when the peak Si strain reaches $\varepsilon_{\text{fracture}}$. As shown in Fig. 9, the compressibility decreases almost linearly with increasing prestrain, and vanishes when the maximum applicable pretrain $\frac{\varepsilon_{\text{fracture}}^2}{4\varepsilon_c}\left(1+\frac{43}{48}\frac{\varepsilon_{\text{fracture}}^2}{4\varepsilon_c}\right)$ is reached. Therefore the compressibility is well approximately by $\frac{\varepsilon_{\text{fracture}}^2}{4\varepsilon_c}\left(1+\frac{43}{48}\frac{\varepsilon_{\text{fracture}}^2}{4\varepsilon_c}\right)-\varepsilon_{\text{pre}}$. Fig. 9 also shows the strechability $\varepsilon_{\text{pre}}+\varepsilon_{\text{fracture}}+\varepsilon_c$. As the prestrain increases, the stretchability improves but the compressibility worsens. Such a figure is useful for the design of Si thin films in stretchable electronics. For example, if a Si thin film/PDMS substrate system has equal stretchability/compressibility, then the prestrain is about 13.4%.

7. Concluding remarks

We have established a finite-deformation buckling theory for stiff thin film on compliant substrates. The perturbation method is used to obtain the analytical solution, and is validated by the finite element method.

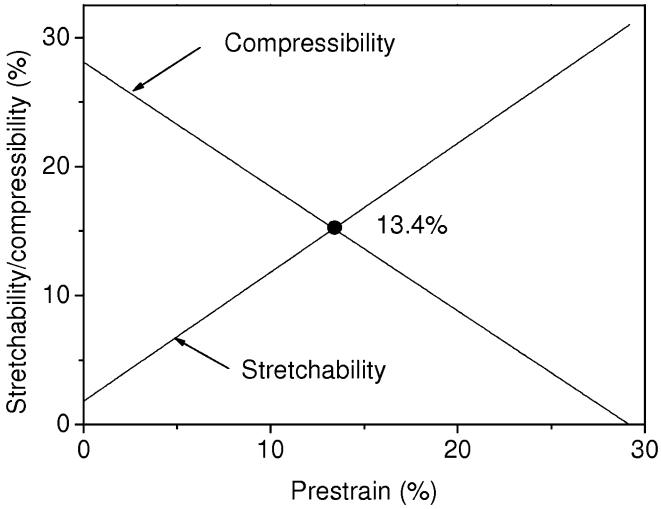

Fig. 9. Strechability and compressibility of buckled structures of Si (100 nm thickness) on PDMS.

Both the analytical solution and numerical results show the strain-dependent buckling wavelength, and agree well with the experiments without any parameter fitting. The strains are accommodated through changes in the amplitudes and wavelengths of buckled geometries. The peak and membrane strains in thin films are obtained analytically, and so are the stretchability and compressibility of the system. These conclusions and the detailed analyses are important for the many envisioned applications for buckled thin film/substrate systems.

Acknowledgements

We acknowledge the support from the National Science Foundation under Grant DMI-0328162, the U.S. Department of Energy, Division of Materials Sciences under Award No. DEFG02-91ER45439, through the Frederick Seitz MRL and Center for Microanalysis of Materials at the University of Illinois at Urbana-Champaign. H.J., Y.H., and Z.J.L., acknowledge the support from NSF CMMI-0700440, NSFC, and the Institute of High Performance Computing in Singapore, respectively.

References

ABAQUS Inc., ABAQUS Analysis User's Manual V6.5 (2004).

Bowden, N., Brittain, S., Evans, A.G., Hutchinson, J.W., Whitesides, G.M., 1998. Spontaneous formation ordered structures in thin films of metals supported on an elastomeric polymer. Nature 393, 146–149.

Bowden, N., Huck, W.T.S., Paul, K.E., Whitesides, G.M., 1999. The controlled formation of ordered, sinusoidal structures by plasma oxidation of an elastomeric polymer. Apply Physics Letters 75, 2557–2559.

Chen, X., Hutchinson, J.W., 2004. Herringbone buckling patterns of compressed thin films on compliant substrates. Journal of Applied Mechanics – Transactions of the ASME 71, 597–603.

Choi, W.M., Song, J., Khang, D.Y., Jiang, H., Huang, Y., Rogers, J.A., 2007. Biaxially stretchable "wavy" silicon nanomembranes. Nano Letters, 71655–71663.

Crawford, G.P., 2005. Flexible Flat Panel Display Technology. John Wiley & Sons, New York.

Efimenko, K., Rackaitis, M., Manias, E., Vaziri, A., Mahadevan, L., Genzer, J., 2005. Nested self-similar wrinkling patterns in skins. Nature Materials 4, 293–297.

Fu, Y.Q., Sanjabi, S., Barber, Z.H., Clyne, T.W., Huang, W.M., Cai, M., Luo, J.K., Flewitt, A.J., Milne, W.I., 2006. Evolution of surface morphology in TiNiCu shape memory thin films. Apply Physics Letters 89, 3.

Harris, A.K., Wild, P., Stopak, D., 1980. Silicon-rubber substrata-new wrinkle in the study of cell locomotion. Science 208, 177–179.

Harrison, C., Stafford, C.M., Zhang, W.H., Karim, A., 2004. Sinusoidal phase grating created by tunably buckled surface. Apply Physics Letters 85, 4016–4018.

Huang, R., 2005. Kinetic wrinkling of an elastic film on a viscoelastic substrate. Journal of the Mechanics and Physics of Solids 53, 63–89.

Huang, R., Suo, Z., 2002. Instability of a compressed elastic film on a viscous layer. International Journal of Solids and Structures 39, 1791–1802.

Huang, Z.Y., Hong, W., Suo, Z., 2005. Nonlinear analyses of wrinkles in a film bonded to a compliant substrate. Journal of the Mechanics and Physics of Solids 53, 2101–2118.

Huck, W.T.S., Bowden, N., Onck, P., Pardoen, T., Hutchinson, J.W., Whitesides, G.M., 2000. Ordering of spontaneously formed buckles on planar surfaces. Langmuir 16, 3497–3501.

INSPEC, 1988. Properties of silicon. Institution of Electrical Engineers, New York.

Jiang, X.Y., Takayama, S., Qian, X.P., Ostuni, E., Wu, H.K., Bowden, N., LeDuc, P., Ingber, D.E., Whitesides, G.M., 2002. Controlling mammalian cell spreading and cytoskeletal arrangement with conveniently fabricated continuous wary features on poly(dimethylsiloxane). Langmuir 18, 3273–3280.

Jiang, H., Khang, D.Y., Song, J., Sun, Y., Huang, Y., Rogers, J.A., 2007. Finite deformation mechanics in buckled thin films on compliant supports. Proceedings of the National Academy of Sciences of the United States of America 104, 15607–15612.

Jin, H.C., Abelson, J.R., Erhardt, M.K., Nuzzo, R.G., 2004. Soft lithographic fabrication of an image sensor array on a curved substrate. Journal of Vacuum Science and Technology B 22, 2548–2551.

Khang, D.Y., Jiang, H.Q., Huang, Y., Rogers, J.A., 2006. A stretchable form of single-crystal silicon for high-performance electronics on rubber substrate. Science 311, 208–212.

Lacour, S.P., Jones, J., Wagner, S., Li, T., Suo, Z., 2004. Stretchable interconnects for elastic electronic surfaces. Proceedings of the IEEE 93, 1459–1467.

Lacour, S.P., Wagner, S., Narayan, R.J., Li, T., Suo, Z., 2006. Stiff subcircuit islands of diamond like carbon for stretchable electronics. Journal of Applied Physics 100, 6.

Lumelsky, V.J., Shur, M.S., Wagner, S., 2001. Sensitive skin. IEEE Sensors Journal 1, 41–51.

Moon, M.-W., Lee, S.H., Sun, J.-Y., Oh, K.H., Vaziri, A., Hutchinson, J.W., 2007. Wrinkled hard skins on polymers created by focused ion beam. Proceedings of the National Academy of Sciences of the United States of America 104, 1130–1133.

Nathan, A., Park, B., Sazonov, A., Tao, S., Chan, I., Servati, P., Karim, K., Charania, T., Striakhilev, D., Ma, Q., Murthy, R.V.R., 2000. Amorphous silicon detector and thin film transistor technology for large-area imaging of X-rays. Microelectronics Journal 31, 883–891.

Schmid, H., Wolf, H., Allenspach, R., Riel, H., Karg, S., Michel, B., Delamarche, E., 2003. Preparation of metallic films on elastomeric stamps and their application for contact processing and contact printing. Advanced Functional Materials 13, 145–153.

Sharp, J.S., Jones, R.A.L., 2002. Micro-buckling as a route towards surface patterning. Advanced Materials 14, 799–802.

Someya, T., Sekitani, T., Iba, S., Kato, Y., Kawaguchi, H., Sakurai, T., 2004. A large-area, flexible pressure sensor matrix with organic field-effect transistors for artificial skin applications. Proceedings of the National Academy of Sciences of the United States of America 101, 9966–9970.

Stafford, C.M., Harrison, C., Beers, K.L., Karim, A., Amis, E.J., Vanlandingham, M.R., Kim, H.C., Volksen, W., Miller, R.D., Simonyi, E.E., 2004. A buckling-based metrology for measure the elastic moduli of polymeric thin films. Nature Materials 3, 545–550.

Stafford, C.M., Vogt, B.D., Harrison, C., Julthongpiput, D., Huang, R., 2006. Elastic moduli of ultrathin amorphous polymer films. Macromolecules 39, 5095–5099.

Sun, Y., Kumar, V., Adesida, I., Rogers, J.A., 2006a. Buckled and wavy ribbons of GaAs for high-performance electronics on elastomeric substrate. Advanced Materials 18, 2857–2862.

Sun, Y., Choi, W.M., Jiang, H., Huang, Y., Rogers, J.A., 2006b. Controlled buckling of semiconductor nano ribbons for stretchable electronics. Nature Nanotechnology 1, 201–207.

Symon, K., 1971. Mechanics. Addison-Wesley, Reading, Mass.

Teixeira, A.I., Abrams, G.A., Bertics, P.J., Murphy, C.J., Nealey, P.F., 2003. Epithelial contact guidance on well-defined micro- and nanostructured substrate. Journal of Cell Science 116, 1881–1892.

Volynskii, A.L., Bazhenov, S., Lebedeva, O.V., Bakeev, N.F., 2000. Mechanical buckling instability of thin coatings deposited on soft polymer substrates. Journal of Material Science 35, 547–554.

Wagner, S., Lacour, S.P., Jones, J., Hsu, P.H.I., Sturm, J.C., Li, T., Suo, Z., 2004. Electronic skin: architecture and components. Physica E 25, 326–334.

Wilder, E.A., Guo, S., Lin-Gibson, S., Fasolka, M.J., Stafford, C.M., 2006. Measuring the modulus of soft polymer networks via a buckling-based metrology. Macromolecules 39, 4138–4143.

Yoo, P.J., Suh, K.Y., Park, S.Y., Lee, H.H., 2002. Physical self-assembly of microstructures by anisotropic buckling. Advanced Materials 14, 1383–1387.